IEEE Access
Multidisciplinary ⋮ Rapid Review ⋮ Open Access Journal

Received 31 July 2026, accepted 13 September 2026, date of publication 17 September 2026,
date of current version 29 September 2026.

Digital Object Identifier 10.1109/ACCESS.2026.3734577

RESEARCH ARTICLE

Demonstration of a Circularly Polarized Antenna Using Self-Biased Ferrite

VINCENT MUZZUPAPA[1], THIERRY MONEDIERE[1], JAMIL FOUANY[2], HERVÉ PARVERY[2], ANTOINE HÖEZ[3], NORBERT PARKER[3], JEAN-LUC MATTEI[3,4], ALEXIS CHEVALIER[3,4], ERIC ARNAUD[1], CYRIL GUINES[1], JOSEPH MUZZUPAPA, AND LAURE HUITEMA[1,5]

[1]Xlim Research Institute, UMR CNRS 7252, University of Limoges, 87060 Limoges, France
[2]CISTEME Company, 87280 Limoges, France
[3]HIT Mag Company, 29280 Brest, France
[4]Lab-STICC Research Institute, UMR CNRS 6285, 29238 Plouzané, France
[5]Institut Universitaire de France (IUF), 75231 Paris, France

Corresponding author: Vincent Muzzupapa (vincent.muzzupapa@xlim.fr)

This work was supported in part by French Defence Innovation Agency (AID) and in part by French National Research Agency (ANR) within the Framework of the CONTACT and CAFÉ Projects under Grant ANR-20-ASTR-0010 and Grant ANR-24-ASTR-0019.

ABSTRACT This paper presents the design, optimization, and experimental validation of a circular patch antenna that leverages a self-biased ferrimagnetic substrate for microwave radiating applications. By utilizing the intrinsic magnetic anisotropy and high permeability of self- biased ferrites, the need for external magnets is eliminated. This enables both circular polarization (CP) and miniaturization without additional biasing hardware. The antenna was optimized by modeling ferrite behavior using the Green and Sandy tensor model used in the case of partially magnetized materials, thereby aligning the minima of the axial ratio (AR) and reflection coefficient (S11) at the same frequency. Experimental results confirm a right-handed circular polarization (RHCP) operation over the 12.8–13 GHz band, achieving an AR of 0.8 dB. The antenna demonstrates a maximum realized gain of 1.55 dB while maintaining a compact form factor of $\lambda 0/6.4 \times \lambda 0/6.4$ at 12.9 GHz. Notably, CP radiation is achieved solely through the properties of the ferrite, removing the need for external electronics or bulky permanent magnets. These findings underscore the potential of self-biased ferrites to enable compact, lightweight, and magnet-free CP antenna systems for advanced microwave applications.

INDEX TERMS Antenna, circular polarization, ferrimagnetic, miniature, self-biased hexaferrite.

I. INTRODUCTION

Circularly polarized waves are of great interest in many fields, since it allows to overcome misalignment drawbacks between an emitting and a receiving antenna, or allows for better signal transmission in complex environments such as multipath mediums, in dense cities for instance, or in depolarizing medium like atmosphere for earth-space transmission or adverse meteorological conditions [1]. For an antenna, circular polarization is typically achieved by exciting two orthogonal field components with a 90° phase difference [2]. One common approach to achieving these conditions involves using multiple feeding ports [3], [4] in order to excite orthogonal modes of the antenna. While effective, this method increases the complexity of the RF back-end, requiring additional components such as phase shifters, extra feed lines, and power dividers. These added elements not only increase the system's weight and footprint but may also contribute to higher insertion losses. In applications where space and weight constraints are critical, this method becomes impractical, and alternative approaches are more desirable. Another way for obtaining circular polarization is to excite orthogonal modes by disturbing the shape of the antenna [5], [6]. While this method avoids increasing system complexity or size, it often leads to reduced bandwidth and distortion of the radiation pattern. Due to the aforementioned limitations and to combine circular polarization and compactness while using a single probe feeding, an attractive solution is

The associate editor coordinating the review of this manuscript and approving it for publication was Su Yan.

© 2026 The Authors. This work is licensed under a Creative Commons Attribution-NonCommercial-NoDerivatives 4.0 License.
For more information, see https://creativecommons.org/licenses/by-nc-nd/4.0/

to use ferrite materials [7]. Indeed, thanks to their anisotropy and their non-reciprocal behavior, ferrites can generate, under a continuous (DC) magnetic bias field, two circular polarized waves presenting an opposite polarization (RHCP and LHCP). This inherent capability offers the potential for a reduced footprint and lower insertion losses. These features have been exploited for the development of circulators [8], [9], isolators [10], [11] and antennas [12], [13].

Ferrites commonly used in RF applications are typically based on iron and yttrium garnets. In order to be magnetized, these soft magnetic materials require the application of an external DC magnetic field, usually provided by bulky permanent magnets, which can hinder compact integration. In this work, a self-biased M-type barium hexaferrite (BaM) is employed for antenna development. The key advantage of using self-biased BaM lies in its ability to eliminate the need for external magnets entirely, thanks to its intrinsic magnetic anisotropy. This property is particularly valuable for the design of miniaturized and integrated RF components.

Although a few studies have investigated self-biased ferrite-based devices, most have focused on circulators [14], [15]. To the best of the authors' knowledge, this is the first paper about a self-biased ferrite being used in a radiating structure. Given the high miniaturization potential of such materials, this work aims to demonstrate their suitability for antenna applications and to exploit their intrinsic properties to enable circular polarization without additional biasing magnets.

Rather than aiming at outperforming existing circularly polarized antenna technologies, the objective of this work is to provide the first experimental demonstration that the intrinsic permeability tensor of a self-biased ferrite can itself generate circularly polarized radiation in a radiating element. As such, this paper should be regarded as a proof of concept establishing the technological feasibility of self-biased ferrite-based circularly polarized antennas and providing the necessary modeling and experimental foundations for future performance-oriented developments.

The first section of the paper provides background on self-biased materials, with an emphasis on RF-relevant parameters such as saturation magnetization (M_s), remanent magnetization (M_R), and magnetocrystalline anisotropy field (H_k). The Green and Sandy tensor model is applied to account for internal demagnetization effects during antenna modeling and optimization. The second section describes the antenna structure along with simulation and design methodology. This is followed by a description of the fabrication steps and a discussion of the measured performance. The paper concludes with a summary of the key findings.

II. ABOUT THE FERRITE

The self-biased ferrite material used in this paper is M-type barium hexaferrite (BaM). For RF applications, the key magnetic parameters of interest are the saturation magnetization (M_S), remanent magnetization (M_R), and the magnetocrystalline anisotropy field (H_K). At the macroscopic scale and in the absence of an external magnetic field, ferrimagnetic materials are composed of regions known as Weiss domains. When a magnetic field is applied, the magnetizations of these domains begin to align. The total magnetization of the material reaches a maximum, defined as the saturation magnetization, when all domains are aligned. The magnetic field required to achieve this state is known as the anisotropy field (H_K); above this threshold, the material is said to be saturated. For field strengths below this threshold, the relationship between the applied field and the resulting magnetization follows the hysteresis behavior illustrated in Fig. 1, which shows a typical hysteresis loop for a ferrimagnetic material.

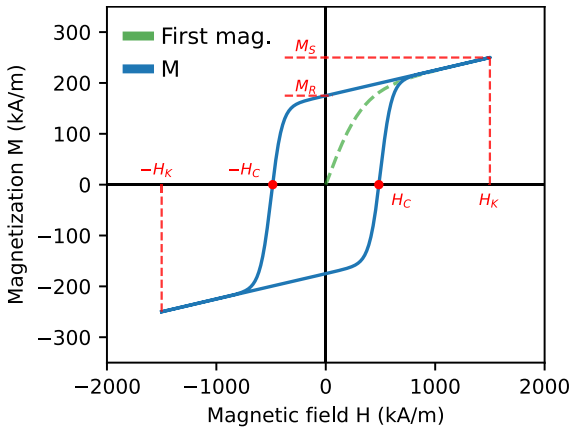

FIGURE 1. Hysteresis cycle of the magnetization of a ferrite.

During the initial magnetization process (depicted by the green curve), magnetization increases with the applied field until it approaches saturation. When the external field is removed, the material retains a non-zero magnetization known as the remanent magnetization Mr. The magnetic field required to bring the magnetization back to zero after the first magnetization is called the coercive field (H_C).

Due to their high remanent magnetization, hexaferrites, such as the M-type barium hexaferrite (BaM) used in this work, can be operated in microwave applications without requiring an external bias field. Thus, using a self-biased ferrite implies that the device operates solely based on the remanent state of the material, offering a significant advantage in terms of integration and compactness by eliminating bulky permanent magnets. When a microwave (RF) field is applied along with a static magnetic field, the permeability of ferrites must be described using a tensorial form, as established in the literature [16]. The appropriate tensor model depends on the magnetization state of the material, and three regimes can be identified: unmagnetized, fully saturated, and partially magnetized. The unmagnetized state exhibits isotropic behavior with negligible anisotropy and is of little relevance here. The fully saturated state, where all Weiss domains are aligned, allows for direct modeling using the Polder tensor [17], a method commonly employed for soft ferrites biased with external magnets. In contrast, the M-type BaM ferrite investigated in this study operates in a

partially magnetized regime, relying solely on its remanent magnetization. In such cases, if the ratio M_R/M_S deviates significantly from unity, the assumptions underlying the Polder model become unaccurate. Instead, more advanced models, such as the Green and Sandy tensor [18], must be used to accurately capture internal demagnetization effects and to ensure reliable antenna modeling and optimization.

Consequently, the ratio Mr/Ms emerges as a key figure of merit. Although a ratio of 1 would be ideal, it is not achievable in practice in the targeted frequency range, due to material limitations. Nonetheless, higher values of this ratio are generally more favorable, as they indicate stronger remanent magnetization and thus more effective self-biased operation. This parameter directly influences the magnetic behavior of the ferrite and guides the selection of suitable models for accurate electromagnetic simulation and antenna design.

The anisotropy field value ($H_K = 17$kOe) of barium hexaferrite ($BaFe_{12}O_{19}$) allows this material to be used in applications operating at about 40-45GHz. In order to adapt this hexaferrite to the present application, which is intended to operate at much lower frequencies, we prepared a polycrystalline sample of the BaM type with the chemical composition $BaFe_{11}Co_{0.5}Ti_{0.5}O_{19}$. We used for this a soft chemistry fabrication method that we have developed [19], [20]. Starting materials were $BaCO_3$, cobalt(II) hydroxide Co(OH)2, titanium(IV) oxide TiO_2, and goethite FeO(OH). Structural characterisations obtained from XRD experiments, together with Curie temperature (T_C) measurement, reveal that only the BaM phase is present. In Ti/Co-doped BaM ferrites, the Curie temperature is approximately 270 °C [21]. Although this value is lower than that of undoped BaM because of reduced exchange interactions, the crystalline structure remains unchanged. Consequently, while the anisotropy field decreases, no significant modification of its temperature dependence is expected. The seminal work reported in [22] demonstrates that BaFe12O19 exhibits only a weak temperature dependence of the anisotropy field, and a similar behavior is therefore expected for the doped ferrite used in this work The substitutions of Ti and Co, combined with the appropriate synthesis process, make it possible to lower the anisotropy field down to $H_K = 11.6$kOe, which corresponds to a GyroMagnetic Resonance (GMR) frequency (f_r) of 32.6GHz. As the antenna is intended to operate around 13GHz, then far from the gyroresonance f_r, this value of H_K seems to be adequate. The obtained material consists of a stack of hexaferrite particles, which confers the sample strong remanent magnetisation. Finally, the material is characterized by a high coercive field $H_C = 1.77$ kG, which provides strong immunity against external magnetic perturbations and contributes to the stability of the self-biased operating state. The magnetic properties of the M-type barium hexaferrite (BaM) of radius a and height h used in this work are summarized in TABLE 1.

With ΔH the resonance line width modeling the magnetic losses of the material.

TABLE 1. Magnetic and geometric properties of the M-Type barium hexaferrite $BaFe_{11}Co_{0.5}Ti_{0.5}O_{19}$ used in this work.

M_S (kG)	M_R (kG)	$\frac{M_R}{M_S}$	ε_r	ΔH (kOe)	H_K (kOe)	H_C (kG)	T_C (°C)	f_r (GHz)	a (mm)	h (mm)
3.15	2.8	0.89	16	0.5	11.66	1.77	270	32.6	3.61	0.2

In our specific case, the bulk ferrite material exhibits an intrinsic Mr/Ms ratio of 0.89, which is relatively high and could, under ideal conditions, justify modeling the material as fully saturated using the Polder tensor. However, the actual geometry of our sample, a cylindrical ferrite with a radius of 3.61 mm and a thickness of 0.2 mm, introduces significant demagnetizing effects [22], [23]. These effects substantially reduce the effective magnetization, lowering the Mr/Ms ratio to approximately 0.48. At such reduced level, the saturated-state assumption becomes invalid. Therefore, in this work, we adopt the model proposed by Green and Sandy [18], whose permeability tensor is presented in (1).

$$[\mu] = \begin{bmatrix} \mu & -j\kappa & 0 \\ j\kappa & \mu & 0 \\ 0 & 0 & \mu_z \end{bmatrix} \tag{1}$$

With $\mu = \mu' - j\mu''$ and $\mu_z = \mu'_z - j\mu''_z$ represent the complex diagonal, and $\kappa = \kappa' - j\kappa''$ the complex off diagonal element of the permeability tensor. The real parts of these components are defined as follows:

$$\mu' = \mu'_0 + (1 - \mu'_0)\left(\frac{M_r}{M_s}\right)^{\frac{3}{2}} \tag{2}$$

$$\kappa' = \frac{\gamma 4\pi M_r}{\omega} \tag{3}$$

$$\mu'_z = \mu'_0\left(1 - \frac{M_r}{M_s}\right)^{\frac{5}{2}} \tag{4}$$

With

$$\mu'_0 = \frac{2}{3}\left[1 - \left(\frac{\gamma 4\pi M_s}{\omega}\right)^2\right]^{\frac{1}{2}} + \frac{1}{3} \quad \text{and} \quad \omega = 2\pi f \tag{5}$$

With γ the gyromagnetic ratio ($\gamma = 2.8$ MHz/Oe).

Furthermore, it is important to note that in the Green-Sandy model, material losses, represented by the imaginary parts of the components of the permeability tensor, are not taken into account and are assumed to be zero; that is, $\mu'' = 0$, $\mu''_z = 0$ and $\kappa'' = 0$. However, since losses cannot be ignored during the antenna optimization process, we have assumed that the losses are those described by Polder's tensor model, as given in equations (6), (7) and (8)

$$\mu'' = \mu''_z = \frac{\alpha\omega\omega_m(\omega_r^2 + \omega^2(1 - \alpha^2))}{(\omega_r{}^2 - \omega^2(1 + \alpha^2))^2 + 4\alpha^2\omega_r{}^2\omega^2} \tag{6}$$

$$\kappa'' = \frac{2\alpha\omega^2\omega_r\omega_m}{(\omega_r{}^2 - \omega^2(1 + \alpha^2))^2 + 4\alpha^2\omega_r{}^2\omega^2} \tag{7}$$

With

$$\alpha = \frac{\gamma \Delta H}{2f}, \omega_m = 2\pi\gamma M_s, \omega_r = \omega_0 + j\alpha\omega \tag{8}$$

With α a damping factor representing magnetic losses.

In the remainder of this paper, we present the design of a circularly polarized radiating element based on the self-biased ferrite introduced in this section, whose characteristics are summarized in Table 1. One of the main objectives of this work is to investigate the potential of self-biased ferrites for low-frequency microwave applications. The principal limitation of such materials lies in their intrinsically strong anisotropy field, which results in a high GMR frequency and a gyrotropic response that rapidly decreases below this resonance. To investigate the feasibility of operating at lower frequencies, the proposed antenna was intentionally designed to operate well below the GMR of the developed ferrite. This operating regime represents a realistic design scenario in which the device specifications are driven by the targeted application rather than by the material properties. Consequently, the antenna performance reflects the compromises associated with the material characteristics instead of relying on operation close to the optimum gyrotropic conditions. For the developed ferrite, the GMR occurs at 32.6 GHz, whereas the antenna was designed to operate around 13 GHz.

III. MODAL ANALYSIS

In order to understand the impact of the Mr/Ms ratio on the microwave performance of a device, and thereby assess the influence of using a self-biased hexaferrite material, a modal study can be conducted, starting from the solutions of the propagation equation for TM modes within a cylindrical ferrite cavity of radius a=3.6mm [12], [24]:

$$J_n'(ka) \pm n.\frac{\kappa}{ka\mu} J_n(ka) = 0 \tag{9}$$

With

$$k = \omega\sqrt{\mu_{eff}\,\varepsilon} \quad \text{and} \quad \mu_{eff} = \frac{\mu^2 - \kappa^2}{\kappa^2} \tag{10}$$

where J_n is the Bessel function of the first kind of order n, J_n' its first order derivative, a the radius of the ferrite, k the wave number, μ_{eff} the effective permeability, and κ and μ are the elements of the permeability tensor. For the present design, consistent with our earlier ferrite antennas that relied on externally biased materials [25], [26], we focus on the fundamental TM_{-11} and TM_{+11} cavity modes, because they yield a broadside radiation pattern while radiating right-hand or left-hand circular polarization, respectively. Specifically, the $n = -1$ mode produces RHCP and the $n = +1$ mode produces LHCP. The resonant frequencies of these two modes, obtained from the roots of the propagation equation (9), can lie very close to one another; their separation depends on the anisotropy factor κ'/μ', which in turn depends on both the distance from the GMR and the quality of the magnetization, represented by the M_R/M_S ratio. Fig. 2 presents Equation (9) evaluated near its first root for both $n = \pm 1$ modes and for various values of the M_R/M_S ratio, illustrating how the remanent-to-saturation magnetization ratio influences the separation between modal resonant frequencies.

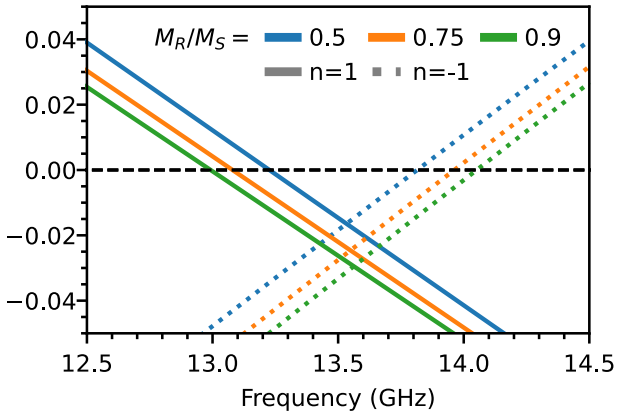

FIGURE 2. Plot of the solutions of the propagation equation in the ferrite cavity using Green and Sandy's model.

Increasing the M_R/M_S ratio widens the frequency separation between the TM_{-11} (RHCP) and TM_{+11} (LHCP) resonances, which is advantageous for achieving high-quality circular polarization. Because the two modes radiate with opposite handedness, a mid-band region exists where their fields couple and the opposite polarizations tend to cancel, degrading the response toward linear polarization. For antenna applications, it is therefore desirable to maximize the modal spacing to preserve the widest possible circular-polarization bandwidth around each resonance. In the present work, because of the relatively low $M_R/M_S = 0.48$ and the operation far from the GMR, the modal separation obtained is approximately 590 MHz around 13.51 GHz. Although this separation is sufficient to experimentally demonstrate, for the first time, the feasibility of using a self-biased ferrite in a circularly polarized antenna, it remains relatively small, and consequently a limited axial-ratio bandwidth is expected.

IV. ANTENNA'S ARCHITECTURE

The architecture of the proposed circularly polarized patch antenna, based on the previously presented self- biased ferrite cavity, follows a conventional aperture-coupled patch configuration. The antenna comprises two main elements: the ferrite and the dielectric substrate. The ferrite has a cylindrical shape with a diameter of 3.61 mm and a thickness of 200 μm. Its top surface is gold-plated (1 μm thick). The ferrite exhibits a relative permittivity of $\varepsilon_r = 16$ and a low dielectric loss tangent of approximately $tg(\delta) \approx 10^{-4}$. Its magnetic properties have been discussed in the previous section. Further details on the fabrication and characterization of this material can be found in [19]. The antenna structure, illustrated in Fig. 3, is built on a 320 μm-thick alumina substrate that supports both the feeding network and the coupling mechanism. A metallic ground plane is deposited on the upper

surface of the substrate, serving as the lower boundary of the ferrite cavity. A coupling slot is etched into this ground plane to enable energy transfer from the microstrip feed line to the ferrite-loaded cavity. The metallized cylindrical ferrite is positioned directly above the slot. On the bottom side of the alumina substrate, a combination of Co-Planar Waveguide (CPW) and microstrip line, connected via a tapered transition [27], is employed for feeding. Although single microstrip lines are typically used in aperture-coupled designs [28], [29], the inclusion of a CPW section in this design offers several advantages: it reduces conduction losses, eliminates the undesirable back radiation usually associated with microstrip feeds, and facilitates antenna characterization using Ground-Signal-Ground (GSG) probes. The CPW section begins at the edge of the substrate and extends inward, transitioning into the microstrip line several millimeters before the slot. The microstrip continues beyond the slot and terminates in an open circuit, forming a shunt stub. The length of this stub is carefully optimized to achieve impedance matching with a standard 50 Ω feed.

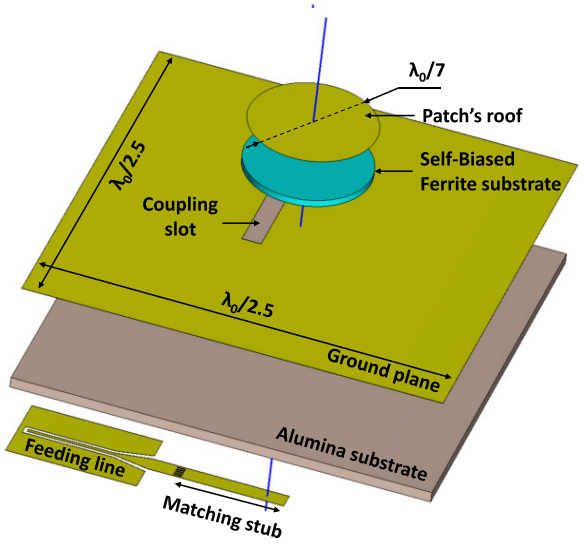

FIGURE 3. Exploded view of the antenna's architecture. Schematic is not on scale.

V. SIMULATION AND OPTIMIZATION

The simulations were conducted using CST Studio Suite, with the ferrite modeled as a fully tensor-defined material, allowing all nine components of both the permittivity (ε) and permeability (μ) tensors to be specified. The elements of the $[\mu]$ tensor were defined according to the Green and Sandy model [10], as recalled in the previous section, using the measured remanent and saturation magnetization values (M_R and M_S) listed in TABLE 1. Since the Green and Sandy model does not inherently account for magnetic losses, imaginary components were assumed to be those derived from Polder's tensor, as previously discussed.

Moreover, when the device operates far from the gyromagnetic resonance frequency, the loss factor α is defined as a function of the effective magnetic linewidth ΔH_{eff} according to $\alpha = \gamma.\Delta H_{eff}/(2f)$ [30], where γ is the gyromagnetic ratio and f is the operating frequency. In this case, the antenna operates around 13 GHz, which is significantly lower than the gyromagnetic resonance frequency of 32.6 GHz. Consequently, ΔH_{eff} is the relevant parameter for accurately modeling magnetic losses. In the specific case of the self- biased ferrite developed in this work, we considered $\Delta H_{eff} = 25$ Oe.

All simulations employed open (add space) boundary conditions to accurately capture radiation effects, and the structure was excited using a waveguide port. As an initial validation, the ferrite cavity was simulated with a discrete port to identify its natural resonant modes. The circularly polarized modes were observed as minima in the axial ratio (AR) at 12.42 GHz and 12.95 GHz, respectively, as shown in Fig. 4. While slightly downshifted, these results are consistent with the analytical predictions from the propagation equation in Section II (13.24 GHz and 13.8 GHz). This difference can be explained by the fact that the analytical model approximates magnetic walls at the ferrite periphery (for r=a).

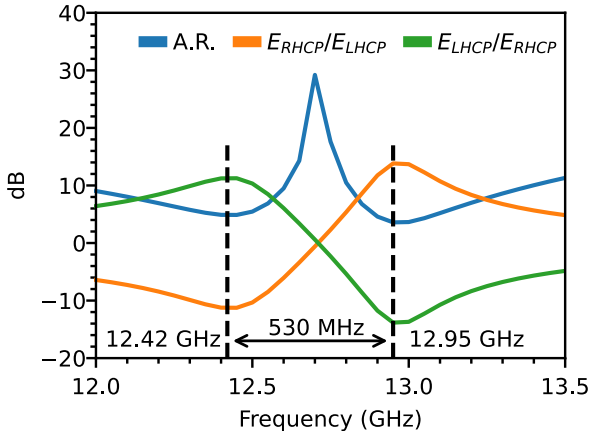

FIGURE 4. Resonant modes of the single ferrite cavity excited by a discret port. Axial Ratio is taken in the $\varphi = 0°$ and $\theta = 0°$ direction.

Moreover, the 530 MHz frequency separation observed between the two modes is in good agreement with the analytical prediction (590 MHz). Furthermore, the order of mode appearance is corroborated by evaluating the ratios between the left-hand circular polarization (LHCP) and right-hand circular polarization (RHCP) components of the electric field. As the second mode (RHCP) exhibits a lower AR, antenna optimization efforts were subsequently focused on impedance matching for this mode.

A second simulation was conducted by introducing the coupling slot into the ground plane and incorporating a 50 Ω microstrip line of arbitrary length onto the alumina substrate. The microstrip line extends 1 mm before and 2.5 mm beyond the slot, terminating in an open circuit. The structure is excited using a waveguide port placed at the beginning of the microstrip line. To isolate the impact of the slot position on the coupling efficiency, the slot, microstrip line, and

waveguide port were translated together across the ground plane in the $\hat{y}$-direction, maintaining their relative alignment. The slot's length-to-width ratio was fixed at 10:1, a configuration commonly adopted in aperture-coupled patch antenna designs [28], [31]. Due to the radial symmetry of the ferrite cavity, the slot was moved solely along the radial $\hat{y}$-direction, as illustrated in Fig. 5.

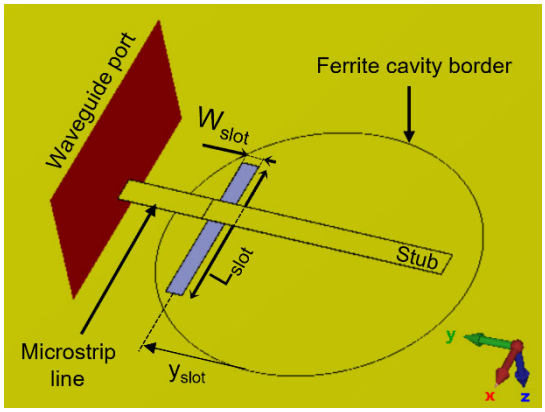

FIGURE 5. Simulation model used for optimizing slot dimensions and position.

Fig. 6 presents the simulated front-to-back radiation ratio (FBRR), a key parameter for two main reasons. First, it effectively quantifies the coupling efficiency between the feeding line and the resonant cavity in this class of antenna architectures. Second, since the length of the open-circuited stub can range from 0 to $\lambda_g/2$, it may itself become radiative, which is an effect that must be minimized. A higher FBRR indicates stronger coupling into the ferrite cavity and reduced unwanted radiation from the feeding structure. The FBRR was evaluated for slot's lengths (L_{slot}) ranging from 1 mm to 2 mm and for slot's positions (y_{slot}) varying from 0 mm (slot centered in the ferrite cavity) up to 1.3 mm along the $\hat{y}$ axis. These ranges were selected to ensure that the slot remains entirely within the footprint of the ferrite cylinder. According to the simulation results shown in Fig. 6, the optimal coupling configuration is achieved for the longest slot (2 mm) positioned at the maximum tested offset from the center (1.3 mm), yielding the highest FBRR. Indeed, for this configuration, the front gain exceeds the back gain by 8.6 dB. However, the FBRR is not the only parameter to consider, as antenna performance also strongly depends on impedance matching. A common criterion is to ensure that $|S_{11}| < -10$ dB at the operating frequency, indicating good input matching. Based on the FBRR trends observed in 6, we selected the range of slot lengths where FBRR is highest and analyzed the corresponding input impedance behavior. Specifically, the slot position was fixed at 1.3 mm from the cavity center, since this offset consistently yields the best FBRR. Within this configuration, only slot lengths greater than 1.6 mm and up to 2.0 mm were considered, ensuring strong coupling while keeping the slot inside the footprint of the ferrite cylinder. Fig. 7 presents the simulated complex input impedance for three slot lengths within this range. It can be observed that the resonant frequency slightly shifts with varying slot length. As the slot lengthens, the frequency of the impedance peak decreases and tends to move away from the frequency at which the AR is minimum, which remains close to 12.95 GHz. To ensure optimal alignment between the impedance resonance and the point of best circular polarization, the slot length was set to 1.85 mm. This configuration provides a good compromise, offering a favorable FBRR of 7.6 dB while maintaining the resonance close to the minimum AR.

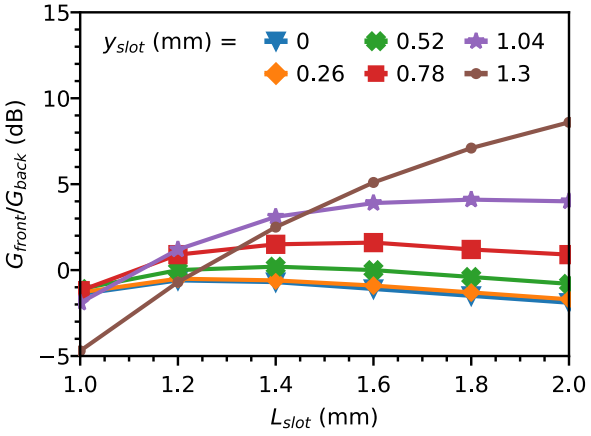

FIGURE 6. Front-to-back radiation ratio used to discriminate different configurations of the coupling slot.

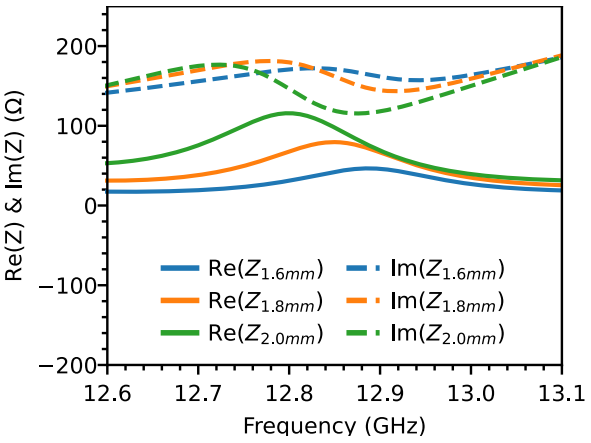

FIGURE 7. Simulated input impedance for different slot's length.

In the previous parametric study, the slot width (W_{slot}) was maintained at one-tenth of its length. To investigate the influence of slot width independently, an additional parametric analysis was conducted while fixing the length at the previously optimized value of 1.85 mm. As shown in Fig. 8, increasing the slot's width exhibits a similar trend to increasing its length: the wider the slot, the higher the front-to-back radiation ratios (FBRR), indicating improved coupling efficiency. However, while FBRR is an important metric, particular attention has been paid to the effect of the slot's width on the AR, an essential parameter for

characterizing circular polarization. Fig. 9 presents the AR variation over frequency for different slot's widths. Although the 200 μm-wide slot achieves the highest FBRR, it also results in the narrowest 3 dB AR bandwidth (170 MHz) and the highest AR value (2.28 dB at 12.95 GHz). In contrast, the 150 μm-wide slot offers a wider AR bandwidth (240 MHz, a 40% improvement) and reduces the minimum AR down to 0.5 dB at the same frequency, albeit the FBRR is slightly reduced (6.7 dB).

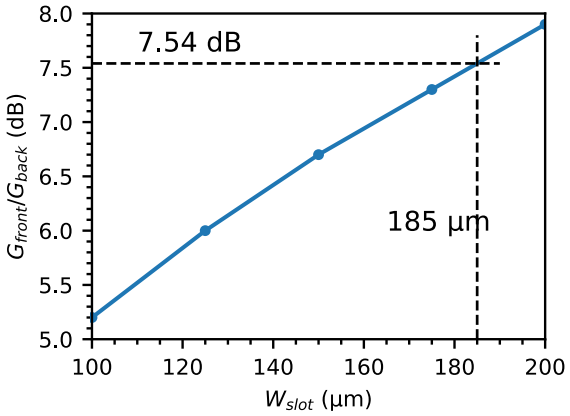

FIGURE 8. Front-to-back radiation ratio over slot's width.

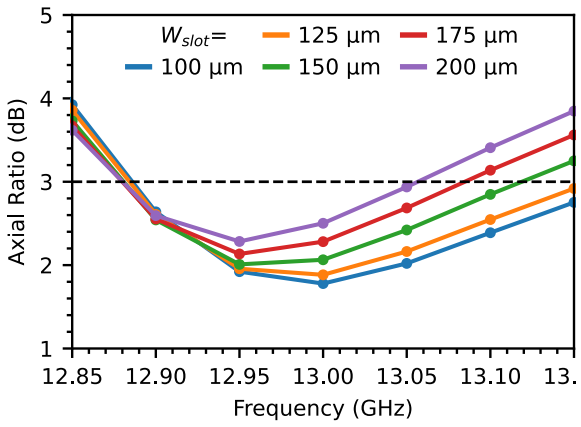

FIGURE 9. Axial Ratio over frequency for different slot's widths.

Despite this trade-off, an FBRR of 6.7 dB still indicates that the antenna radiates approximately 4.6 times more power in the forward direction than in the backward direction. Therefore, the slot length was fixed at 150 μm to balance circular polarization quality and coupling efficiency. Following the slot dimensioning, a parametric study was conducted on the length of the microstrip stub to achieve impedance matching to 50 Ω. Since the input impedance along a transmission line is periodic with a period of $\lambda_g/2$ [32], the stub length was swept from 0 to $\lambda_g/2$ (approximately 5 mm). Fig. 10 presents the simulated evolution of both the real and imaginary components of the input impedance as a function of stub length.

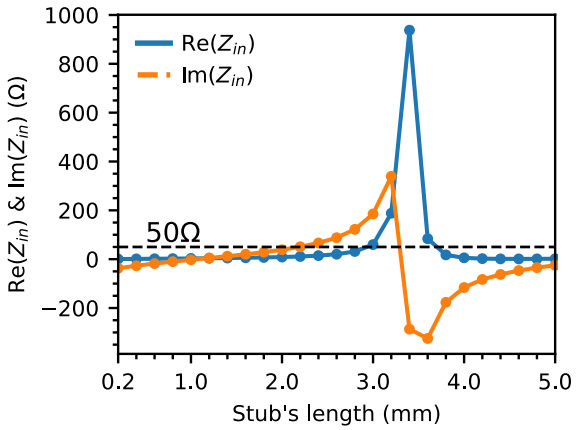

FIGURE 10. Real and imaginary parts of the simulated input impedance over the stub's length at 12.95 GHz.

From Fig. 10, it is evident that varying the stub length alone does not allow the input impedance to reach 50 Ω. The impedance can either exhibit a low reactance combined with a very small resistance, or a resistance close to 50 Ω with a high reactance. The latter scenario is more favourable, as the high reactance can be compensated by adding a series capacitor. To achieve this, a series capacitance can be inserted along the microstrip line between the feeding port and the coupling slot. The stub length was set to 2.9 mm, resulting in an input impedance of approximately 50 + j162 Ω. Since the capacitor is connected in series, its reactance must be equal in magnitude to the input reactance, i.e., $|Z_c| = 162\ \Omega$, which corresponds to a capacitance of around 76 fF. This value was then confirmed through schematic-level simulation in CST. The corresponding results are presented in Fig.11.

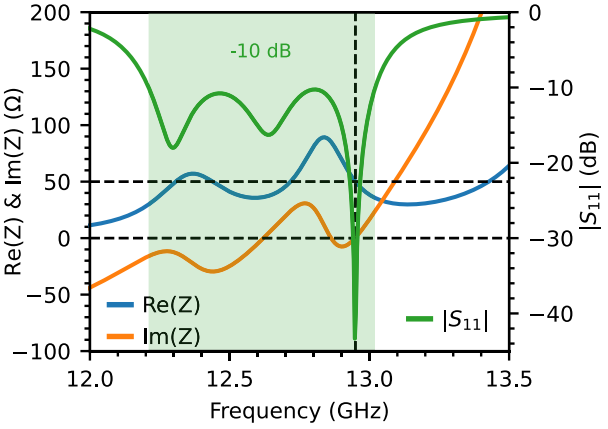

FIGURE 11. Simulated input impedance with serial capacitance of 76 fF.

The schematic-level simulation predicts excellent impedance matching centered at 12.95 GHz, corresponding to the frequency where the AR reaches its minimum. A capacitance value of approximately 79 fF is required, which can be realized using a localized structure on the microstrip line rather than a surface-mounted component (SMD). Specifically, an interdigitated capacitor (IDC) can be integrated

directly into the microstrip excitation line, at the location of the previously defined waveguide port. The design methodology for such capacitors has been previously presented in the literature [33]. To ensure integration compatibility, the total width of the IDC was fixed at 300 μm to match the width of the microstrip line. The finger length is limited to 100 micrometers in order to reduce conductor losses. Starting from an initial sizing based on analytical formulas from [34], an optimization was performed on both the finger width and the spacing between fingers. The resulting dimensions that achieve the desired capacitance are summarized in TABLE 2.

To complete the antenna model, which is intended for measurement using Ground Signal Ground probes, a transition from coplanar waveguide to microstrip topology is also included and illustrated in Fig. 12. This transition was designed according to the guidelines presented in [27]. The full dimensions of the final antenna structure are provided in TABLE 2.

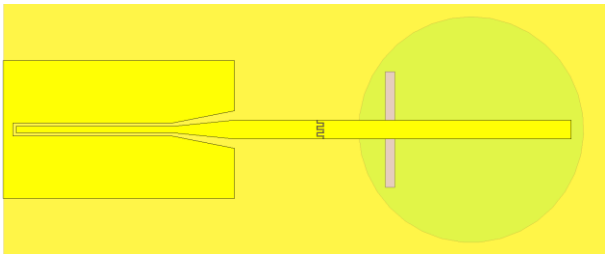

FIGURE 12. Bottom view of the complete CST model of the overall antenna.

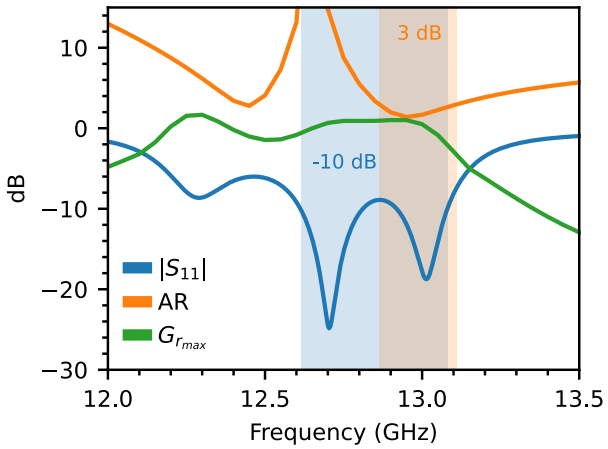

FIGURE 13. Simulated performances of the antenna.

Fig. 13 presents the full-wave simulation results, incorporating all previously described elements of the antenna. The simulated device demonstrates a $|S_{11}|$ below -10 dB over a bandwidth of 400 MHz, spanning from 12.62 GHz to 13.08 GHz. The 3 dB AR bandwidth is 250 MHz, extending from 12.86 GHz to 13.11 GHz. The effective operational bandwidth, defined as the frequency range satisfying both criteria, is therefore 220 MHz, between 12.86 GHz and 13.08 GHz. Within this band, the maximum realized gain ranges from -2 dB to 1.06 dB. These values are obtained with a $\Delta H_{eff} = 25$ Oe.

TABLE 2. Dimensions of the overall antenna device.

	W (µm)	Gap (µm)	L (mm)	Position (mm)	Thickness (µm)
CPW	100	53	2.5	/	5
Transition	300	150	1	/	5
Microstrip	300	/	1.157[1]	/	5
Slot	1850	/	150	1300[2]	5
IDC (fingers)	42	12.5	100	1.029[3]	5
Stub	300	/	2.9	0[4]	5
Substrate	1500	/	1500	/	315-320

[1] total length on both sides of the IDC, [2] from ferrite toward the CPW, [3] from center of the slot toward the CPW, [4] from center of the slot backward the CPW

VI. FABRICATION PROCESS OF THE ANTENNA

The complete antenna device consists of three main components: the alumina substrate (featuring the slotted ground plane and feeding line), the ferrite (described in Section II), and a Rohacell holder that ensures proper alignment and mechanical stability of the structure. The ferrite element is a flat cylindrical sample of $BaFe_{12-2x}Co_xTi_xO_{19}$ with x=0.4, fabricated using the process detailed in [19]. A 1 μm-thick gold layer was subsequently deposited on its top surface via electron-beam physical vapor deposition (PVD). The ferrite cavity is defined by this metallized cylindrical ferrite placed over the slotted ground plane deposited on the alumina substrate. Fabrication of the alumina-based feeding structure begins with the deposition of a 25/300 nm Ti/Au bilayer on both sides of a 1-inch × 1-inch alumina substrate using PVD. Electrical isolation between the two sides was verified before proceeding. Gold layers on each side were then electroplated up to a final thickness of 5 μm, with the substrate periodically rotated during the process to ensure uniform growth. Photolithographic patterning of the ground slot and feeding line was carried out using AZ nLof 2020 (negative resist) and Dow S1813 (positive resist), respectively. The patterns were exposed using a Kloe Dilase 650 laser writer. Metal etching was performed using a Bi-sublimed iodine/potassium iodide solution for gold, and a Buffered Oxide Etch (BOE 7:1, HNO_3 68%) for titanium. Following etching, the photoresist was stripped, and the substrate was cut to its final dimensions of 15 mm × 15 mm. The final component of the overall device is the mechanical holder, fabricated from Rohacell HF 71 [19] using a 3-axis CNC milling machine. This structure serves two primary functions: to accurately align the ferrite above the slot etched in the ground plane, and to apply pressure to eliminate any air gap within the resonant cavity. The overall view of the antenna holder is shown in Fig. 14 and photographs of the fabricated antenna are presented in Fig. 15, with and without the holder. In Fig. 15 (b), the stud and the ferrite has been temporarily removed to reveal the slotted ground plane.

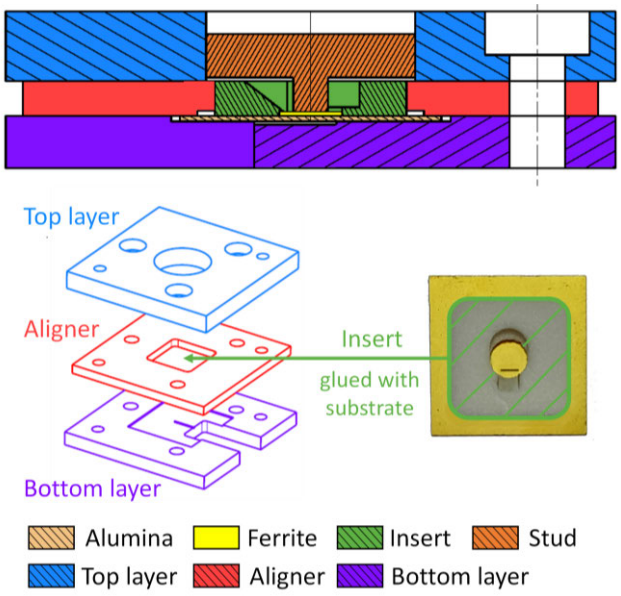

FIGURE 14. Overall view of the antenna's holder.

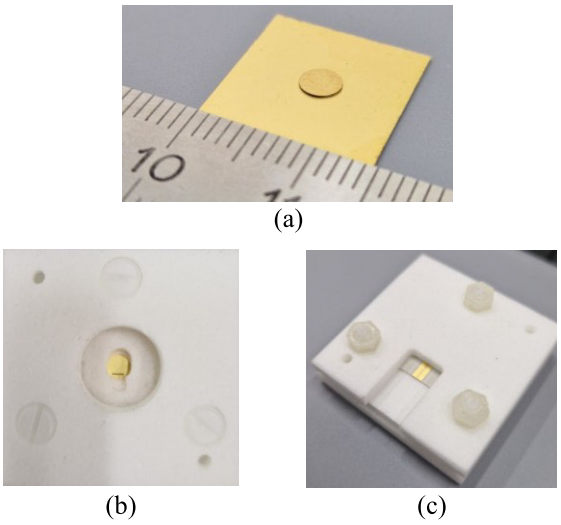

FIGURE 15. Photographs of the fabricated antenna: (a) self-biased ferrite mounted on the alumina-based slotted ground plane, (b) Rohacell holder without the stud and ferrite temporarily removed to reveal the slot in the ground plane, and (c) fully assembled device ready for measurement using GSG probes.

VII. MEASUREMENT RESULTS AND DISCUSSION

The antenna's performance was evaluated using a 3D scanner developed at the XLIM research institute, as shown in Fig. 16. This scanner enables probe-based measurements (Ground-Signal-Ground configuration) in a semi-anechoic environment. Fig. 17 presents the measured $|S_{11}|$ parameter and the boresight AR. The measured $|S_{11}|$ closely matches the simulated results, with only a minor frequency shift of approximately 180 MHz (1.4 %) downward. Consequently, the measured -10 dB impedance bandwidth ranges from 12.41 GHz to 12.99 GHz. The measured 3D boresight AR exhibits a 3 dB bandwidth of 170 MHz between 12.82 GHz and 12.99 GHz, with a minimum AR value of 0.8 dB at 12.95 GHz These results demonstrate that an axial ratio below 3 dB can be experimentally achieved even when operating well below the gyromagnetic resonance. The operating band defined by the $|S_{11}| < -10$ dB and AR < 3 dB criteria is thus 170 MHz wide, between 12.82 GHz and 12.99 GHz.

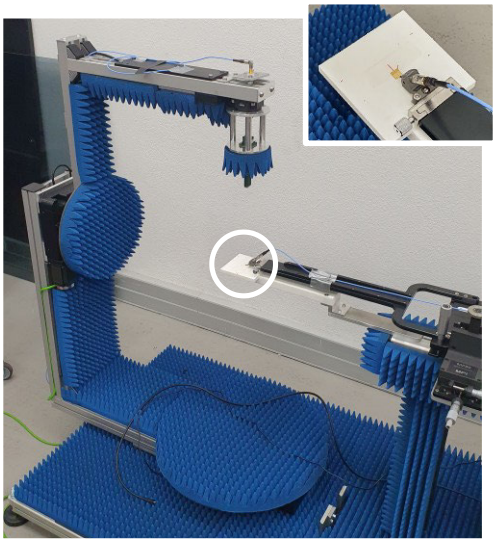

FIGURE 16. 3D scanner used to measure the antenna.

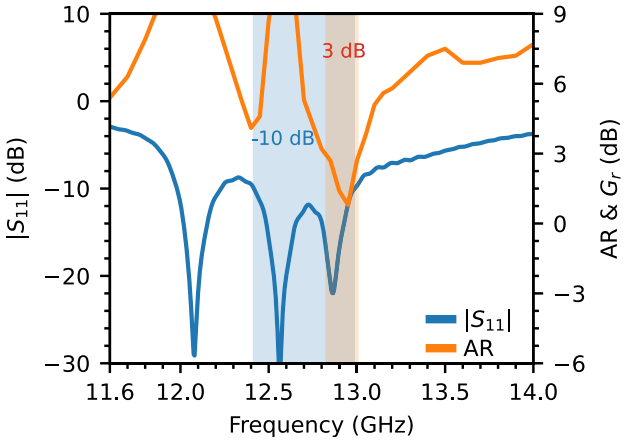

FIGURE 17. Measured reflection coefficient and boresight AR of the antenna.

Within this frequency range, the maximum measured RHCP realized gain (Fig. 18) varies from -0.1 dB up to 1.45 dB, while the corresponding cross-polarization discrimination (XPD) reaches 22 dB. This demonstrates that the RHCP component clearly dominates the LHCP component, confirming the generation of a high-quality right-hand circularly polarized wave.

The relatively low realized gain of the proposed antenna is mainly attributed to its very low profile ($\lambda_0/116$). To support this interpretation, the measured RHCP realized gain is compared in Fig. 19 with simulated realized gain obtained for the fabricated antenna (ferrite thickness of 0.2 mm), while the simulations are extended to ferrite substrate thicknesses ranging from 0.2 mm to 0.7 mm. It can be clearly observed

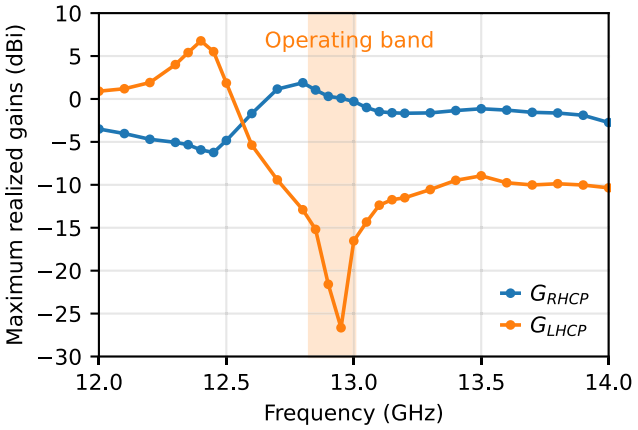

FIGURE 18. Measured maximum RHCP and LHCP realized gains of the antenna.

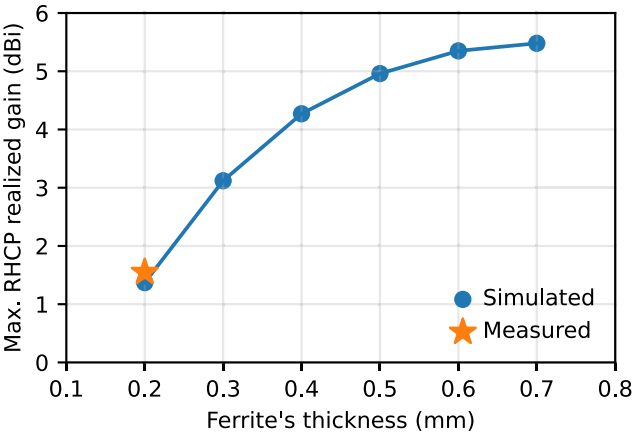

FIGURE 19. Comparison between measured (h=0.2 mm) and simulated RHCP realized fain for different ferrite thicknesses.

that the realized gain increases with the ferrite thickness. In particular, increasing the ferrite substrate thickness from 200 μm to 600 μm improves the simulated realized gain by approximately 4 dB. This result confirms that the limited realized gain measured on the fabricated prototype is primarily related to the available substrate thickness rather than to the self-biased ferrite concept itself. Therefore, future devices, no longer constrained by the current ferrite mold thickness, are expected to achieve significantly higher realized gain values. Together with the accurate modeling of the permeability tensor and its implementation in full-wave electromagnetic simulations, these results provide the first experimental demonstration of the feasibility of designing radiating elements based on self-biased ferrites. They establish a solid foundation for future performance optimization and demonstrate the capability of the proposed material to naturally generate circularly polarized radiation through its intrinsic permeability tensor.

These results confirm the robustness of the proposed approach and highlights the potential of using self-biased ferrite to achieve circular polarization with very satisfactory gains, marking an important first step toward practical applications. Finally, the left and right measured realized gains are plotted in Fig. 20. in the planes $\varphi = 0°$ and $\varphi = 90°$ at 12.9 GHz.

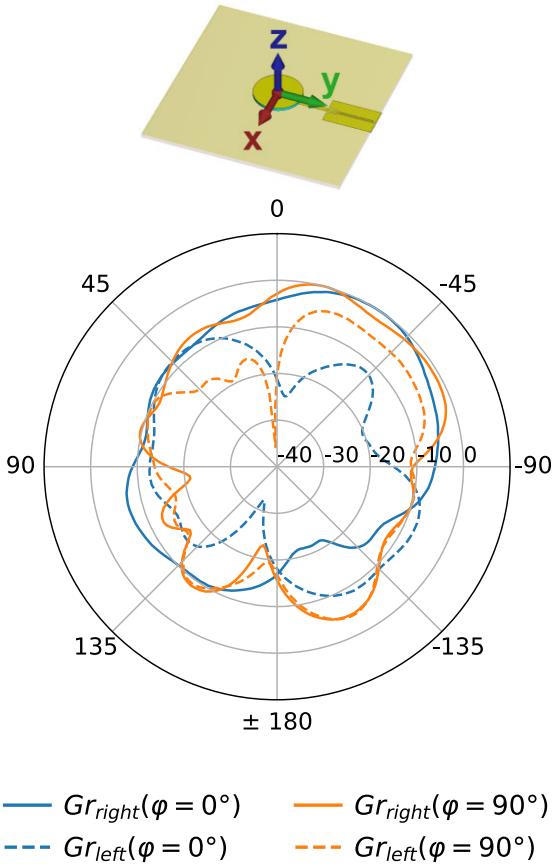

FIGURE 20. Normalized measured radiation patterns (left and right realized gains) of the antenna in the $\varphi = 0°$, 90° planes at 12.9 GHz.

The measured radiation exhibits the expected steering effects, which are consistent with the measurement environment (presence of the probes and semi-anechoic conditions). Importantly, these results provide the first experimental validation of a circularly polarized antenna using self-biased ferrite, demonstrating both feasibility and promising performance.

To place the proposed device in the context of the state of the art, TABLE 3 compares its performance with that of recently reported circularly polarized antennas based on different technological approaches. The effective bandwidth is defined here as the frequency range over which the impedance-matching and 3-dB axial-ratio bandwidths overlap.

The comparison shows that the proposed antenna provides a competitive trade-off between compact dimensions and effective bandwidth, particularly considering its very low profile. The compactness of the proposed device is directly related to the use of a self-biased ferrite, which eliminates the need for external permanent magnets placed around the ferrite substrate, as required in conventional externally biased ferrite antennas. Moreover, compared with conventional CP

TABLE 3. Comparison with other technologies of circularly polarized antennas.

Ref.	Technology	$f_{central}$	Effective BW* (% / MHz)	Gain (dBi)	Electrical dimensions (W×L×H)
[3]	90° Hybrid coupler	3.65	8.2 / 295	2	0.81×0.4×0.02
[35]	90° Hybrid coupler	11.2	3.15 / 353	12.5	3.7×3.7×0.057
[36]	Asymetric radiator	2.52	14.5 / 365	4.35	1.25×1.25×0.04
[37]	45° feed	2.54	1.2 / 30	10.3	1.27×1.27×0.03
[38]	Phase-change material	29.5	1.7 / 400	6.2	1.23×1.23×0.03
[25]	Externally Biased ferrite	2.42	4.1 / 100	-9.6	0.16×0.16×0.076
**[26]	Externally Biased ferrite	Multi.	2 / X	2.7	Sphere of radius 0.15
**[39]	Externally Biased ferrite	Multi.	2.5 / X	0.9	0.38×0.34×0.033
This work	**Self-biased ferrite**	**12.9**	**1.4 / 180**	**1.45**	**0.6×0.6×0.009**

* Combining $|S_{11}| < -10$ dB and A.R.< 3 dB
** Multi-band devices. Presented performances are averaged, and should be checked directly in the articles

antenna solutions based on couplers, multiple feeding paths, or asymmetric radiating structures, the proposed antenna relies on the intrinsic permeability tensor of the self-biased ferrite to generate circularly polarized radiation, resulting in a particularly compact radiating structure without the need for additional circuit.

Although the effective bandwidth remains limited in this first proof-of-concept device, several strategies can be considered for further improvement. Operation closer to the gyromagnetic resonance to increase the anisotropy factor, the use of ferrite materials with a lower anisotropy field to shift the gyromagnetic resonance toward lower frequencies can directly enhance the circular polarization bandwidth, or operation in the negative effective permeability region could significantly increase the axial-ratio bandwidth [39]. These different operating regimes involve specific trade-offs, particularly in terms of impedance matching, and can be investigated for designs targeting specific applications.

VIII. CONCLUSION

In this paper, we have demonstrated for the first time the use of a self-biased ferrite in a radiating device, allowing to generate circularly polarized waves from a simple and compact design. Thanks to the intrinsic anisotropic behavior of the ferrite, no additional feed or radiator shaping was required to achieve circular polarization. In the same time, its high effective permittivity and permeability for significant size reduction, making the antenna electrically small ($\frac{\lambda_0}{1.7} \times \frac{\lambda_0}{1.7} \times \frac{\lambda_0}{116}$). Combined with the elimination of bulky external magnets, this results in a highly compact solution.

The close agreement between measured and simulated resonant frequencies of the RHCP mode, as well as the consistency of the realized gain, validates the proposed modeling approach. The fabricated prototype operates from 12.82 GHz to 12.99 GHz, achieving a minimum axial ratio of 0.8 dB and a maximum realized gain of 1.45 dB. The relatively low value of gain compared with conventional circularly polarized patch is mainly explained by the very low profile ($\lambda_0/116$) of the antenna imposed by the ferrite substrate's mold.

Overall, this pioneering proof-of-concept highlights the potential of self-biased hexaferrites to enable compact, magnet-free, and efficient circularly polarized antennas, opening new perspectives for advanced multifunctional antenna designs.

ACKNOWLEDGMENT

This work benefited from the support of the PLATINOM platform (www.unilim.fr\) and the PILIM Program The PLATINOM test facility of XLIM is a member of the CNRS RF-Net network (ANR-22-PEFT-0011).

REFERENCES

[1] P. Nepa, F. Cavallo, M. Bonaccorsi, M. Aquilano, M. C. Carrozza, and P. Dario, "Experimental analysis of RSSI-based indoor location systems with WLAN circularly polarized antennas," in *Wireless Mobile Communication and Healthcare* (Lecture Notes of the Institute for Computer Sciences, Social Informatics and Telecommunications Engineering), vol. 55. Berlin, Germany: Springer, 2011, pp. 176–183, doi: 10.1007/978-3-642-20865-2_23.

[2] C. A. Balanis, "Fundamental parameters of antennas," in *Antenna Theory: Analysis and Design*, 3rd ed., Hoboken, NJ, USA: Wiley, 2005, p. 1118.

[3] A. H. Mohammed, F. M. Alnahwi, and Y. I. A. Al-Yasir, "A circularly polarized microstrip antenna with dual circular polarization using a 90° hybrid coupler and proximity-coupled feeding for LTE 43 5G applications," *Appl. Sci.*, vol. 14, no. 24, p. 11877, Dec. 2024, doi: 10.3390/app142411877.

[4] W. Wang, C. Chen, and W. Wu, "Low-profile dual-band dual circularly polarized patch antenna with small frequency ratio," *Int. J. RF Microw. Comput.-Aided Eng.*, vol. 31, no. 10, 2021, Art. no. e22806, doi: 10.1002/mmce.22806.

[5] S.-S. Hao, Q.-Q. Chen, J.-Y. Li, and J. Xie, "A high-gain circularly polarized slotted patch antenna," *IEEE Antennas Wireless Propag. Lett.*, vol. 19, no. 6, pp. 1022–1026, Jun. 2020, doi: 10.1109/LAWP.2020.2987330.

[6] K. Y. Lam, K.-M. Luk, K. F. Lee, H. Wong, and K. B. Ng, "Small circularly polarized U-slot wideband patch antenna," *IEEE Antennas Wireless Propag. Lett.*, vol. 10, pp. 87–90, 2011, doi: 10.1109/LAWP.2011.2110631.

[7] J. Helszajn, *Principles of Microwave Ferrite Engineering*. New York, NY, USA: Wiley, 1969.

[8] V. Olivier, L. Huitema, B. Lenoir, H. Turki, C. Breuil, P. Pouliguen, and T. Monediere, "Dual-band ferrite circulators operating on weak field conditions: Design methodology and bandwidths' improvement," *IEEE Trans. Microw. Theory Techn.*, vol. 68, no. 7, pp. 2521–2530, Jul. 2020, doi: 10.1109/TMTT.2020.2988003.

[9] L. Marzall, D. Psychogiou, and Z. Popovic, "Microstrip ferrite circulator design with control of magnetization distribution," *IEEE Trans. Microw. Theory Techn.*, vol. 69, no. 2, pp. 1217–1226, Feb. 2021, doi: 10.1109/TMTT.2020.3045995.

[10] L. Zeng, C.-Y.-E. Tong, and S. N. Paine, "A low-insertion loss cryogenic edge-mode isolator with 18 GHz bandwidth," *IEEE J. Microw.*, vol. 3, no. 4, pp. 1258–1266, Oct. 2023, doi: 10.1109/JMW.2023.3307297.

[11] S. Khim, J. L. Valdes, H. Parvery, L. Huitema, and T. Monediere, "Planar isolator based on field displacement in ferrite substrate," in *Proc. 54th Eur. Microw. Conf. (EuMC)*, Sep. 2024, pp. 172–175, doi: 10.23919/EUMC61614.2024.10732277.

[12] D. M. Pozar, "Radiation and scattering characteristics of microstrip antennas on normally biased ferrite substrates," *IEEE Trans. Antennas Propag.*, vol. 40, no. 9, pp. 1084–1092, Sep. 1992, doi: 10.1109/8.166534.
[13] T. Wang, H. Zhai, J. Li, and Q. Sun, "Ferrite-loaded magnetically reconfigurable SIW magnetic dipole antenna with tunable frequencies," *IEEE Antennas Wireless Propag. Lett.*, vol. 23, no. 10, pp. 2969–2973, Oct. 2024, doi: 10.1109/LAWP.2024.3416521.
[14] N. Parker-Soues, N. Noutehou, C. Patris, D. Nevo, J. L. Mattei, R. Lebourgeois, O. Vendier, J. L. Roux, and V. Laur, "Compact self-biased Q-band circulators," *IEEE Trans. Magn.*, vol. 57, no. 4, pp. 1–6, Apr. 2021, doi: 10.1109/TMAG.2021.3059946.
[15] W. M. Gitzel, S. Bahadori Rad, M. Heidenreich, J. Töpfer, and A. F. Jacob, "Integration concept for a self-biased Ka-band circulator," in *Proc. 23rd Int. Microw. Radar Conf. (MIKON)*, Oct. 2020, pp. 350–352, doi: 10.23919/MIKON48703.2020.9253784.
[16] R. E. Collin, "Microwave propagation in ferrites," in *Foundations for Microwave Engineering*, 2nd ed., Hoboken, NJ, USA: Wiley, 2001, pp. 450–460.
[17] D. Polder, "VIII. On the theory of ferromagnetic resonance," *London, Edinburgh, Dublin Phil. Mag. J. Sci.*, vol. 40, no. 300, pp. 99–115, Jan. 1949, doi: 10.1080/14786444908561215.
[18] J. J. Green and F. Sandy, "Microwave characterization of partially magnetized ferrites," *IEEE Trans. Microw. Theory Techn.*, vol. MTT-22, no. 6, pp. 641–645, Jun. 1974, doi: 10.1109/TMTT.1974.1128306.
[19] A. Hoëz, J.-L. Mattei, and A. Chevalier, "New manufacturing process for granular texture management in polycrystalline BaM hexaferrites through the goethite crystallite laths aspect ratio, and a specialized law of approach to the magnetic saturation for partly polarized uniaxial materials," *Magnetochemistry*, vol. 9, no. 1, p. 30, Jan. 2023, doi: 10.3390/magnetochemistry9010030.
[20] A. Hoez, J.-L. Mattei, and A. Chevalier, "Experimental determination of anisotropy fields, first and second anisotropy constants, and remanent magnetizations in self-polarized Zn–Ti and Co–Ti equally co-substituted BaM ferrites," *IEEE Trans. Magn.*, vol. 59, no. 11, pp. 1–5, Nov. 2023, doi: 10.1109/TMAG.2023.3282604.
[21] T. Tsutaoka and N. Koga, "Magnetic phase transitions in substituted barium ferrites $BaFe_{12-x}(Ti_{0.5}Co_{0.5})_xO_{19}$ (x=0−5)," *J. Magn. Magn. Mater.*, vol. 325, pp. 36–41, Jan. 2013, doi: 10.1016/j.jmmm.2012.07.050.
[22] B. T. Shirk and W. R. Buessem, "Temperature dependence of M_s and K_1 of $BaFe_{12}O_{19}$ and $SrFe_{12}O_{19}$ single crystals," *J. Appl. Phys.*, vol. 40, no. 3, pp. 1294–1296, Mar. 1969, doi: 10.1063/1.1657636.
[23] M. S. Sodha and N. C. Srivastava, "1.8. dipole-dipole interaction: Demagnetization," in *Microwave Propagation in Ferrimagnetics*, vol. 1981. Boston, MA, USA: Springer, 1981, pp. 33–43.
[24] J. Ghalibafan, B. Rejaei, and N. Komjani, "A circularly polarized antenna based on the unidirectional resonant modes of a ferrite disk," *IEEE Trans. Magn.*, vol. 50, no. 3, pp. 88–95, Mar. 2014, doi: 10.1109/TMAG.2013.2283655.
[25] S. Jemmeli, T. Monediere, E. Arnaud, and L. Huitema, "Ultra-miniature and circularly polarized ferrite patch antenna," *IEEE Trans. Antennas Propag.*, vol. 71, no. 8, pp. 6435–6443, Aug. 2023, doi: 10.1109/TAP.2023.3284166.
[26] S. Jemmeli, T. Monediere, E. Arnaud, and L. Huitema, "Design of a miniature circularly polarized antenna operating in three frequency bands using a polarized ferrite material," *IEEE Trans. Antennas Propag.*, vol. 69, no. 8, pp. 4304–4312, Aug. 2021, doi: 10.1109/TAP.2020.3045756.
[27] G. Zheng, J. Papapolymerou, and M. M. Tentzeris, "Wideband coplanar waveguide RF probe pad to microstrip transitions without via holes," *IEEE Microw. Wireless Compon. Lett.*, vol. 13, no. 12, pp. 544–546, Dec. 2003, doi: 10.1109/LMWC.2003.820638.
[28] D. Sun, W. Dou, and L. You, "A wideband aperture-coupled microstrip patch antenna with backed cavity of dielectric," in *Proc. 9th Int. Symp. Antennas, Propag. EM Theory*, Nov. 2010, pp. 226–228, doi: 10.1109/ISAPE.2010.5696439.
[29] D. M. Pozar, "Microstrip antenna aperture-coupled to a microstripline," *Electron. Lett.*, vol. 21, no. 2, pp. 49–50, Jan. 1985, doi: 10.1049/el:19850034.
[30] J. Helszajn, "Tensor permeability in a magnetic insulator," in *The Stripline Circulator: Theory and Practice*. Hoboken, NJ, USA: Wiley, 2008, pp. 27–30.
[31] J. P. Kim, "Optimum design of an aperture-coupled microstrip patch antenna," *Microw. Opt. Technol. Lett.*, vol. 39, no. 1, pp. 75–78, Oct. 2003, doi: 10.1002/mop.11132.
[32] D. M. Pozar, "Transmission line theory," in *Microwave Engineering*, 4th ed., Hoboken, NJ, USA: Wiley, 2012, pp. 451–496.
[33] V. Muzzupapa, A. Crunteanu, E. Arnaud, D. Passerieux, C. Borderon, and L. Huitema, "Frequency tunable millimeter-wave patch antenna integrating ferroelectric capacitors," *IEEE Access*, vol. 13, pp. 152115–152130, 2025, doi: 10.1109/ACCESS.2025.3600868.
[34] F. Jean, L. Huitema, A. Ghalem, M. Rammal, A. Boulle, F. Rémondière, J.-C. Orlianges, S. Députier, A. Crunteanu, D. Passerieux, M. Chatras, M. Guilloux- Viry, and J.-R. Duclère, "Microwave dielectric properties of pure and Mn-doped lead-free $Na_{0.5}Bi_{0.5}TiO_3$ epitaxial thin films grown on (001) $LaAlO_3$ single crystals using pulsed laser deposition: Microwave dielectric properties of pure and Mn-doped $Na_{0.5}Bi_{0.5}TiO_3$ layers," *Phys. Status Solidi (A)*, vol. 213, no. 12, pp. 3221–3230, Dec. 2016, doi: 10.1002/pssa.201600209.
[35] P. Squadrito, S. Zhang, and G. F. Pedersen, "X-band dual circularly polarized patch antenna with high gain for small satellites," *IEEE Access*, vol. 7, pp. 74925–74930, 2019, doi: 10.1109/ACCESS.2019.2921088.
[36] J. Yu, B.-Y. Shi, and Z.-M. Chen, "Microstrip ring sector dual-circularly polarized antenna with tilted beams," *IEEE Access*, vol. 13, pp. 203370–203377, 2025, doi: 10.1109/ACCESS.2025.3639148.
[37] X. Zhang and L. Zhu, "High-gain circularly polarized microstrip patch antenna with loading of shorting pins," *IEEE Trans. Antennas Propag.*, vol. 64, no. 6, pp. 2172–2178, Jun. 2016, doi: 10.1109/TAP.2016.2552544.
[38] J. L. Valdes, L. Huitema, E. Arnaud, D. Passerieux, and A. Crunteanu, "A polarization reconfigurable patch antenna in the millimeter-waves domain using optical control of phase change materials," *IEEE Open J. Antennas Propag.*, vol. 1, pp. 224–232, 2020, doi: 10.1109/OJAP.2020.2996767.
[39] J. Leon Valdes, T. Monédière, E. Arnaud, S. Jemmeli, and L. Huitema, "Multiband circularly polarized ferrite antenna operating with negative effective permeability," *IEEE Trans. Antennas Propag.*, vol. 73, no. 12, pp. 9710–9720, Dec. 2025, doi: 10.1109/TAP.2025.3611684.

VINCENT MUZZUPAPA received the M.S. degree in electronic and telecommunications from Nice University, France, in 2020, and the Ph.D. degree in telecommunication high frequencies from Limoges University, France, in 2024. Since 2024, he has been a Postdoctoral Fellow at the Xlim research institute within the Antennas and Signals Team, University of Limoges. His field of research covers reconfigurable and miniature and millimeter-wave antennas. He is currently working on self-biased ferrite based antennas.

THIERRY MONEDIERE was born in Tulle, France, in 1964. He received the Ph.D. degree from the IRCOM Laboratory, University of Limoges, Limoges, France. He is currently a Professor with the Antennas and Signals Team, Xlim Research Laboratory, University of Limoges. He develops his research activities in this laboratory and works on multifunction antennas, miniature antennas, antenna arrays, and also active antennas. He also studies gyromagnetic devices as ferrite circulators or isolators.

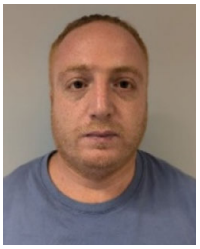

JAMIL FOUANY received the M.S. degree in electronic and optical engineering for high-frequency communications and the Ph.D. degree in telecommunication high frequencies from the University of Limoges, France, in 2012 and 2015, respectively. From 2015 to 2018, he was a Postdoctoral Fellow at the XLIM Research Institute, University of Limoges. He served as the Signal Integrity Team Lead at Multilane, Lebanon, from 2018 to 2022, and is currently a Research Engineer at CISTEME, Limoges, France. His research interests include reconfigurable, millimeter-wave, ferrite, reflector, parasitic element, and nanosatellite antennas, with a focus on advanced high-frequency antenna design and applications.

HERVÉ PARVERY was born in 1975. He received the Ph.D. degree from the University of Limoges. Since 2002, he has been at the Research Lab (Inria/Insa Lyon) and industrial companies (Radiall Systems, Valeo) on RF and antennas topics. Since 2018, he has been at Cisteme as the Co-Leader of the RF components Team. Its activities are mainly focused on the development of antenna systems for RF devices, such as radars, the IoT, telecommunications for example. He provides RF trainings to industrial partners to improve their skills on these subjects.

ANTOINE HÖEZ received the M.Sc. degree in materials science and the Ph.D. degree in condensed matter chemistry and physics from the University of Caen, France, in 2017 and 2021, respectively. He then spent three years as a Postdoctoral Researcher working on the development of new hexaferrite permanent magnets for motor and telecommunications applications. He is the Project Initiator of the startup HITMag, where he currently serves as the Research and Development Director. HITMag develops new permanent magnets.

NORBERT PARKER, photograph and biography not available at the time of publication.

JEAN-LUC MATTEI is currently an Associate Professor at the University of West Brittany (France). He is also with the Lab-STICC Research Laboratory, France, and with HIT Mag company. His current research activities focus mainly on magnetic materials (soft and hard cerzmics): their synthesis methods, and their applications particularly in the microwave field (miniaturized and reconfigurable antennas, self-polarized hexaferrites for non-reciprocal devices).

ALEXIS CHEVALIER received the Ph.D. degree in electronics from the University of Brest, France, in 1998, for his contributions in characterization and modelling of microwave propagation in composite materials. He worked in a Telecom Industry for several years and then he joined the University of Brest, in 2003. He is currently an Associate Professor with the Lab-STICC Laboratory, Brest. His research interests include the electromagnetic properties of materials for microwave engineering. He focuses on developing new measurement methods and models to characterize and predict microwave properties of heterogeneous, anisotropic, absorbing, and dielectric or magnetic materials.

ERIC ARNAUD was born in France, in 1970. He received the Diplôme D'Etudes Supérieures Specialisées (DESS) and Ph.D. degrees in electronics and telecommunication from the University of Limoges, in 1994 and 2010, respectively. He did his Ph.D. on circularly polarized EBG antenna. From 1996 to 2001, he has been an In Charge of the Microwave part of Free-Electron Laser (L.U.R.E). Since 2001, he has been an In Charge of XLIM Laboratory's antenna test range. He participated in several research projects related to the design, development and characterization of antennas. His research interests are mainly in the fields of circularly polarized antenna, agile electromagnetic band gap matrix antenna, and isoflux pattern antenna.

CYRIL GUINES was born in France, in 1987. He received the bachelor's degree in radio frequency and optical systems for telecommunications from the University of Limoges, in 2009. He is the Head of PLATINOM's Micro and Nano-technologies division and participates in several research projects related to the design, development and characterization of RF components and microsystems for telecommunications. He is an In Charge of developing and optimizing micro- and nanotechnology processes for prototyping components and microsystems, such as filters, phase shifters, RF MEMS, antennas, and microfluidic sensors in a clean room environment.

JOSEPH MUZZUPAPA was born in Toulon, France, in 1965. He received the two-year degree in mechanical and production engineering, in 1988, the bachelor's degree in industrial production engineering, in 2008, and the M.S. degree in aeronautics design, in 2019. After that, he begins his career at the Atelier Industriel de l'Aéronautique (AIA) of Cuers-Pierrefeu as a Designer of the Mechanical Design Office for military aeronautics. In 2014, for proposing an innovative concept, he was declared an Inventor for the Ministry Defence of France (https://www.inpi.fr/sites/default/files/import/bopis/bopi1206.pdf). Since 2005, he has also been involved in teaching through partnerships with INSA Lyon and the Mechanical and Production Department, Toulon University Institute of Technology, with the aim of raising students' awareness of advances in industrial methods, particularly GPS coordinates. He stopped his career at AIA, in June 2025, and is currently retired.

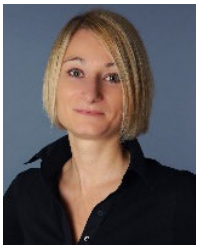

LAURE HUITEMA received the M.S. and Ph.D. degrees in telecommunications high frequencies and optics from Limoges University, in 2008 and 2011, respectively.

From 2011 to 2012, she was a Postdoctoral Research Fellow at the Atomic Energy Commission (CEA), Laboratory of Electronics and Information Technology (LETI), Grenoble, France. She is currently an Associate Professor in the Antennas and Signals Team within the RF systems axis of the XLIM Research Institute, University of Limoges, France. Since 2024, she has been with the Institut Universitaire de France (IUF). Her research interests include reconfigurable antennas, dielectric resonator antennas, miniature antennas, multiband antennas, and circulators. More recently, she has been working on the integration of new components based on innovative materials for their integration into antennas, and was the project leader of a European H2020 project MASTERS (http://www.unilim.fr/H2020_MASTERS/). Project Since 2019, she has been the Director of the Joint Laboratory INOGYRO which groups together the Xlim laboratory and the company Inoveos (https://inogyro.xlim.fr/). She received the Best Student Paper Award at the IEEE International Workshop on Antenna Technology (IWAT) 2010 and the Best Student Paper Award at the JCMM 2010 Conference. In 2020, she was also awarded the Bronze Medal of French National Centre for Scientific Research (CNRS).